

High-fidelity, broadband stimulated-Brillouin-scattering-based slow light using fast noise modulation

Yunhui Zhu,^{1,*} Myungjun Lee,² Mark A. Neifeld,²
and Daniel J. Gauthier¹

¹*Dept. of Physics, Duke University and the Fitzpatrick Institute for Photonics, Durham, NC, 27708, USA*

²*Dept. of Electrical Computer Engineering, University of Arizona, Tucson, AZ, 85721, USA*

[*yunhui.zhu@duke.edu](mailto:yunhui.zhu@duke.edu)

Abstract: We demonstrate a 5-GHz-broadband tunable slow-light device based on stimulated Brillouin scattering in a standard highly-nonlinear optical fiber pumped by a noise-current-modulated laser beam. The noise-modulation waveform uses an optimized pseudo-random distribution of the laser drive voltage to obtain an optimal flat-topped gain profile, which minimizes the pulse distortion and maximizes pulse delay for a given pump power. In comparison with a previous slow-modulation method, eye-diagram and signal-to-noise ratio (SNR) analysis show that this broadband slow-light technique significantly increases the fidelity of a delayed data sequence, while maintaining the delay performance. A fractional delay of 0.81 with a SNR of 5.2 is achieved at the pump power of 350 mW using a 2-km-long highly nonlinear fiber with the fast noise-modulation method, demonstrating a 50% increase in eye-opening and a 36% increase in SNR in the comparison.

© 2011 Optical Society of America

OCIS codes: (060.4370) Nonlinear optics, fibers; (190.5890) Scattering, stimulated; (230.1150) All-optical devices.

References and links

1. R. W. Boyd and D. J. Gauthier, "Controlling the velocity of light pulses," *Science* **326**, 1074–1077 (2009).
2. L. Thévenaz, "Slow and fast light in optical fibres," *Nat. Photonics* **2**, 474–481 (2008).
3. M. González Herráez, K. Y. Song, and L. Thévenaz, "Optically controlled slow and fast light in optical fibers using stimulated Brillouin scattering," *Appl. Phys. Lett.* **87**, 081113 (2005).
4. K. Y. Song and K. Hotate, "25 GHz bandwidth Brillouin slow light in optical fibers," *Opt. Lett.* **32**, 217–219 (2007).
5. T. Sakamoto, T. Yamamoto, K. Shiraki, and T. Kurashima, "Low distortion slow light in flat Brillouin gain spectrum by using optical frequency comb," *Opt. Express* **16**, 8026–8032 (2008).
6. M. González Herráez, K. Y. Song, and L. Thévenaz, "Arbitrary-bandwidth Brillouin slow light in optical fibers," *Opt. Express* **14**, 1395–1400 (2006).
7. Z. Zhu, A. M. C. Dawes, D. J. Gauthier, L. Zhang, and A. E. Willner, "Broadband SBS slow light in an optical fiber," *J. Lightwave Technol.* **25**, 201–206 (2007).
8. L. Yi, Y. Jaouen, W. Hu, Y. Su, and S. Bigo, "Improved slow-light performance of 10 Gb/s NRZ, PSBT and DPSK signals in fiber broadband SBS," *Opt. Express* **15**, 16972–16979 (2007).
9. A. Zadok, A. Eyal, and M. Tur, "Extended delay of broadband signals in stimulated Brillouin scattering slow light using synthesized pump chirp," *Opt. Express* **14**, 8498–8505 (2006).
10. E. Cabrera-Granado, O. G. Calderon, S. Melle, and D. J. Gauthier, "Observation of large 10-Gb/s SBS slow light delay with low distortion using an optimized gain profile," *Opt. Express* **16**, 16032–16042 (2008).

11. Y. Zhu, E. Cabrera-Granado, O. G. Calderon, S. Melle, Y. Okawachi, A. L. Gaeta, and D. J. Gauthier, "Competition between the modulation instability and stimulated Brillouin scattering in a broadband slow light device," *J. Opt.* **12**, 104019 (2010).
12. N. A. Olsson, and J. P. Van Der Ziel, "Fibre Brillouin amplifier with electronically controlled bandwidth," *Electron. Lett.* **22**, 488–490 (1986).
13. B. Zhang, L. Yan, L. Zhang, and A. E. Willner, "Multichannel SBS Slow Light Using Spectrally Sliced Incoherent Pumping," *J. Lightwave Technol.* **26**, 3763–3769 (2008).
14. R. Pant, M. D. Stenner, M. A. Neifeld, and D. J. Gauthier, "Optimal pump profile designs for broadband SBS slow-light systems," *Opt. Express* **16**, 2764–2777 (2008).
15. R. S. Tucker, P. C. Ku, and C. J. Chang-Hasnain, "Slow-light optical buffers: capabilities and fundamental limitations," *J. Lightwave Technol.* **23**, 4046 (2005).
16. Z. Bo, L. S. Yan, J. Y. Yang, I. Fazal, and A. E. Willner, "A single slow-light element for independent delay control and synchronization on multiple Gb/s data channels," *IEEE Photon. Technol. Lett.* **19**, 1081–1083 (2007).
17. A. Zadok, H. Shalom, M. Tur, W. D. Cornwell, and I. Andonovic, "Spectral shift and broadening of DFB lasers under direct modulation," *IEEE Photon. Technol. Lett.* **10**, 1709 (1998).
18. M. D. Stenner, M. A. Neifeld, Z. Zhu, A. M. C. Dawes, and D. J. Gauthier, "Distortion management in slow-light pulse delay," *Opt. Express* **13**, 9995–10002 (2005).
19. Z. Zhu, D. J. Gauthier, Y. Okawachi, J. E. Sharping, A. L. Gaeta, R. W. Boyd, and A. E. Willner, "Numerical study of all-optical slow-light delays via stimulated Brillouin scattering in an optical fiber," *J. Opt. Soc. Am. B* **22**, 2378–2384 (2005).
20. R. W. Boyd, *Nonlinear optics* (Academic Press, San Diego, 2008), Ch. 9.
21. R. W. Boyd, K. Rzaewski, and P. Narum, "Noise initiation of stimulated Brillouin scattering," *Phys. Rev. A* **42**, 5514–5521 (1990).
22. A. Kobyakov, M. Sauer, and D. Chowdhury, "Stimulated Brillouin scattering in optical fibers," *Adv. Opt. Photon.* **2**, 1–59 (2010).

1. Introduction

Stimulated-Brillouin-scattering (SBS)-based slow light in room temperature optical fibers has attracted extensive research interest over the past few years [1, 2]. A fiber-based slow light system can controllably delay optical pulses and can operate over the entire transparency window of the fiber [3]. However, the narrow (~ 35 MHz) natural linewidth of the SBS resonance (full width at half magnitude FWHM) in standard single-mode fibers has limited its application to low-data-rate systems. To solve this problem, broadband SBS slow-light techniques were developed [4–11]. Using the well-known Brillouin spectrum broadening technique by direct current modulation of a semiconductor pump laser [12], Gonzalez-Herráez *et al.* increased the SBS bandwidth to ~ 325 MHz [6]. Subsequently, a number of groups have demonstrated broadband SBS slow-light with bandwidths up to tens of GHz [7–11], a data rate compatible with modern optical communication systems. A multi-channel SBS slowlight system has also been demonstrated by using an incoherent pump source and pass it through spectral-slicing filter [13]. In addition to broadening the spectral linewidth of the SBS resonance, a judicious choice of the current modulation waveform can be used to tailor the SBS gain profile, resulting in improved delay performance for the broadband SBS slow light systems [8–11, 14]. The optimal gain profile that improves the pulse delay under constraints of pulse distortion and pump power is a flat-top gain spectrum with sharp edges [9, 10, 14]. These broadband SBS slow light experiments have extended the application of SBS slow light to broadband all-optical communication devices such as data buffering [15] and data packet synchronization [16].

Most previously reported broadband SBS slow light experiments control the spectral SBS gain profile by direct modulation of the pump laser using a periodic modulation waveform [9–11]. The frequency of the waveform is typically chosen to be in the sub-MHz range so that detailed features of the waveform can be reproduced faithfully using an arbitrary waveform generator. However, such periodic modulation result in a intermittent interaction with the signal beam, which may induce fluctuations to the signal. Previous research that focused on averaged pulse delay was not affected by these fluctuations because they were averaged out. Nevertheless, these low-frequency fluctuations reduces the signal-to-noise ratio (SNR) of a delayed data

sequence and degrades fidelity of the device.

To build an optimal high-fidelity broadband SBS slow light system, we develop a systematic procedure to generate a broadband flat-topped SBS gain profile with direct noise current modulation. We compare such a system to a previous slow modulation method in [10] to experimentally demonstrate slow light performance improvement with increased modulation speed. Random noise current modulation has been used in previous research on broadband SBS slow light systems [6–8]. However, due to limited control over the spectral profile, these previous methods generally result in a Gaussian-shaped SBS gain profile. The frequency-dependent gain of a Gaussian profile causes pulse distortion for large delays. Although Yi *et al.* [8] have discussed shaping the pump spectrum by passing a noise waveform through a saturated electronic amplifier, the control over the SBS gain profile is still limited and highly sensitive to the detailed saturation characteristics of the high speed amplifier, which is often hard to characterize. Here, we present an extension of Yi's method in which the noise distribution is arbitrarily controlled. Compared to Yi's work, the method described in this paper is superior because we have complete control over the noise waveform in a way that is easily generalized to any DFB laser used as a pump beam in broadband SBS slow light systems. It will be shown that, by controlling the distribution of the noise waveform, we are able to tune the shape of the SBS gain profile and obtain the best flat-topped profile that optimizes the slow light delay and reduces distortion. We also find that using a noise modulation function with a sampling rate ~ 400 MHz (fast compared to the phonon lifetime (~ 4 ns) in the fiber) substantially stabilizes the optical signal and improves the data fidelity of the broadband SBS slow light system compared to previous slow modulation methods.

The rest of the paper is organized as follows. Section 2 briefly reviews the dynamics of a distributed feedback (DFB) laser under direct current modulation and describes the procedure to obtain a flat-topped SBS gain profile with two different (slow and fast) modulation waveforms. Section 3 describes and compares the delay performance for a 2.5-Gb/s return-to-zero (RZ) data sequence using these two methods and quantifies transmission fidelity by eye-opening (EO) and signal-to-noise ratio measurements. Finally, our conclusions are summarized in Sec. 4.

2. Broadband optimal SBS gain profile design with direct current modulation

In broadband SBS slow light systems, a spectrally broadened laser is used as the pump beam. In our experiment, a modulation voltage $V(t)$ is added to the DC injection current of the DFB laser via a bias-T (input impedance = 50 Ω). The DFB laser spectrum is thereby broadened. Broadening of the laser's spectrum with direct current modulation has been widely used and a quantitative, semiempirical model for the instantaneous spectral shift of the DFB laser output due to direct current modulation $i(t)$ has been established in [17]. The spectral shift $\omega_p(t)$ as a function of time is given by

$$\omega_p(t) = a_0 i(t) - i(t) \otimes h(t), \quad (1)$$

where the first term on the right-hand-side of Eq. (1) represents the linear adiabatic chirp induced by the almost instantaneous current-related changes of the equilibrium carrier density, a_0 is a constant coefficient, and the second term describes the slower thermal chirp, which changes the frequency as a result of temperature-related changes of the refractive index and physical length of the cavity. The thermal chirp is characterized by the convolution of $i(t)$ with the impulse response $h(t) = \sum a_n e^{-t/\tau_n}$, where the different time constants τ_n correspond to thermal conductivities of different layers in the DFB laser. Measurements for our DFB laser reveal that the dominant thermal term has a time constant as short as 7.5 ns [10]. As a result, an analysis of both the thermal and adiabatic chirp is necessary to obtain a precise design of the laser spectrum.

As has been shown in Ref. [14], the SBS gain profile that optimizes slow-light performance under various practical constrains is rectangular-shaped with sharp edges and a flat top. Such a gain profile produces longer delays and reduces pulse distortion. This is because the flat gain profile enables uniform amplification over the different frequency components of the data stream, minimizing the filtering effect and thereby reducing pulse distortion [18]. The rectangular-shaped gain profile also improves the delay. Using the Kramers-Kronig relation, the abrupt-edged gain profile increases the phase shift, which leads to a larger group index and longer delays [9]. Because the broadband SBS gain profile $g(\omega_s)$ (where ω_s is the signal beam frequency) is given by the convolution of the pump spectrum ($I_p(\omega_p)$) with the intrinsic narrow Lorentzian lineshape ($g_0(\omega_s)$) [19], a rectangular-shaped pump laser spectrum with a width much greater than the Lorentzian linewidth produces the desired optimal broadband SBS gain profile.

We start the design of the optimal SBS gain profile by only considering the linear adiabatic term in Eq. (1). In this case, the frequency distribution of the DFB laser is the same as that of the current modulation waveform. This is true when the characteristic time scale of the modulation is faster than any of the time constants of the DFB laser. When the thermal chirp is present, the spectral distribution of the noise must be adjusted using an iterative method, as described below.

To generate the optimal rectangular-shaped pump spectrum, we use a noise waveform

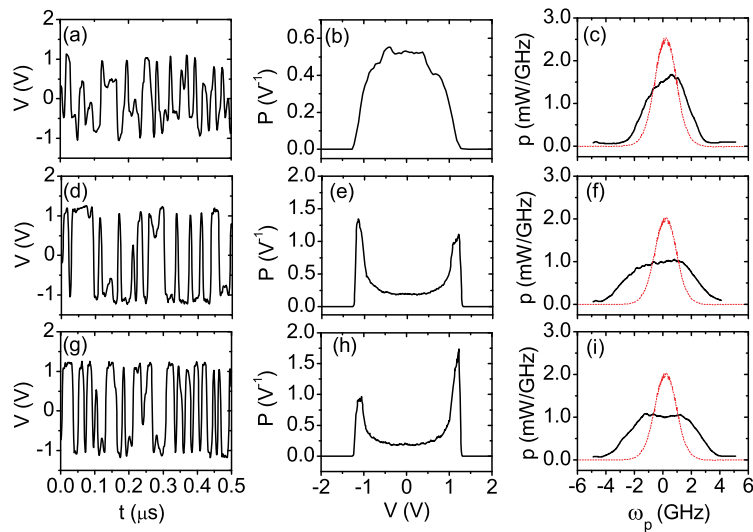


Fig. 1. Pump spectral distribution optimization procedure for the case of fast noise modulation. Modulation voltage waveform $V(t)$ (left column), probability distribution P (bin size = 0.025 V) (middle column) and resultant pump beam spectrum $p(\omega_p)$ (right column) are shown for flat-distributed white noise modulation $V(t) = 2.5 \text{ V} \times f(t)$, where $f(t)$ is a random variable that is approximate uniformly distributed between -0.5 and 0.5 (upper row), bi-peak symmetric noise modulation $V(t) = 2.5 \text{ V} \times \tanh[10f(t)]$ (middle row) and optimal noise modulation $V(t) = 2.5 \text{ V} \times \tanh[10(f(t) + 0.06)]$ (bottom row). A Gaussian spectral profile resulted from a Gaussian noise modulation $V(t) = 2.5 \text{ V} \times g(t)$, where $g(t)$ is a random variable with standard normal distribution, is inserted into the Figs. c, f and i for comparison. The DC injection current is 110 mA.

$V(t) = 2.5 \text{ V} \times f(t)$, in which $f(t)$ is a random variable approximately uniformly distributed between -0.5 and 0.5 (Fig. 1(a)). The sampling time interval is set to 2.5 ns for our arbitrary wavefunction generator (Tektonix AFG3251). Figure 1(b) shows the probability distribution P of the modulation waveform as a function of the voltage V , which is determined from the histogram of the waveform. The spectrum of the pump beam $p(\omega_p)$ is measured by mixing it with a monochromatic reference beam (New Focus Vortex 6029) on a high-speed detector (New Focus Model 1544b), as shown in Fig. 1(c). We see that the generated pump beam spectrum shows significant improvement compared to a Gaussian profile, but is slightly peaked in the center and shows some asymmetry.

The concentration of the spectrum at the center is due to the thermal chirp. In particular, the current of the laser is constantly fluctuating quickly, leading to fluctuations in the temperature about an equilibrium value. According to Eq. (1), a step change in the current $i(t)$ leads to a sudden adiabatic change in the optical frequency $\omega_p(t)$ followed by thermally induced exponential decay to a stationary value. The fast noise-modulation waveform has a rise time ~ 2.5 ns, and has many abrupt changes that can be considered as instantaneous jumps (Fig. 1(a)). After such an abrupt change, the laser spends some time returning towards the previous frequency due to the thermal chirp, which favors frequencies in the middle of the range and causes the center-concentration effect.

To compensate for this effect, we increase the probability distribution in the extrema of the noise distribution, using the function $2.5 \text{ V} \times \tanh(bf(t))$. Figure 1(d)-(f) show the waveform $V(t)$, distribution probability P , and resultant pump spectrum $p(\omega_p)$ for $b = 10$. We see that the center-concentration problem in the pump spectrum is solved, but there is still an asymmetry in the profile, as seen in Fig. 1(f). This asymmetric frequency response is induced by the nonlinear contribution to the adiabatic chirp (not accounted for in Eq. (1)) and the additional different thermal time constants [10]. To solve this problem, an asymmetry is needed in the distribution of the modulation waveform. We use $2.5 \text{ V} \times \tanh[b(f(t) + c)]$, in which the parameter c controls the asymmetry of the distribution.

The best parameter values for an optimal pump spectrum are obtained applying an iterative scheme. As we change the parameters in small steps, the pump spectrum is recorded and compared to an optimal flat-top spectrum. The error (root mean square deviation RMSD) is calculated at each step. After a small number of iterations, we find the combination of parameters that minimizes the error using a steepest descent search procedure, which gives us the optimal values $b = 10$ and $c = 0.06$. As shown in Fig. 1(i), modulation with the optimal parameters results in a good flat-topped spectrum profile with reasonably sharp edges. The RMSD for this spectral profile is 0.164 mW/GHz, compared to 0.25 mW/GHz for Fig. 1(c) and 0.173 mW/GHz for Fig. 1(f).

A similar procedure is used to generate a slow modulation waveform following Cabrera-Granado's approach [10]. We start from a 400-kHz periodic triangular waveform and set the peak to peak amplitude to 2.73 V (Fig. 2(a)). The resultant pump spectrum (Fig. 2(b)) shows a clear asymmetry, which is corrected by introducing a quadratic term in the triangular waveform (Fig. 2(c) and (d)). However, we still observe peaks at the edge of the spectral profile induced by the thermal chirp at the turning points of the waveform. As a result of the thermal chirp, the instantaneous laser frequency spends more time in these regions. These peaks can be corrected by inducing a current "jump" at the turning points, as shown in Fig. 2(e) and (f). The final modulation waveform is expressed as

$$V(t) = v_{\max}/2 \times \begin{cases} at^2 + (4/T - aT/4)t & \text{if } t < T/4 \\ at^2 - (4/T + a3T/4)t + 2 + (2aT^2)/4^2 & \text{if } T/4 < t \leq 3T/4 \\ at^2 + (4/T - a9T/4)t + (5aT^2)/4 - 4 & \text{if } 3T/4 < t \leq T, \end{cases}$$

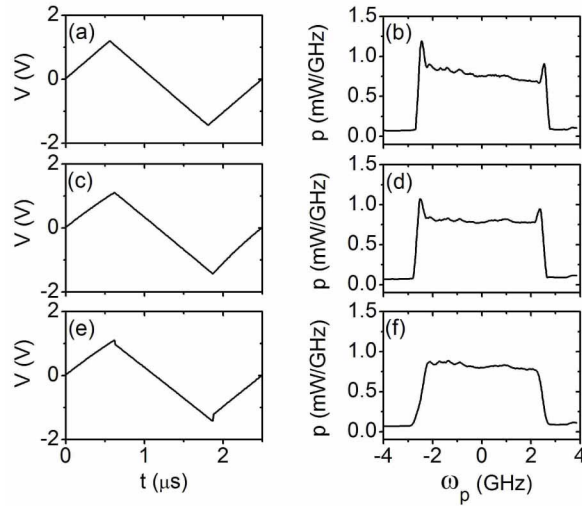


Fig. 2. Pump spectral distribution optimization procedure for the case of slow modulation. Modulation waveform $V(t)$ (left column) and measured pump spectrum profile $p(\omega_p)$ (right column) are shown for triangular modulation (upper row), with the addition of a small quadratic term (middle row), and for the optimum waveform (lower row). The DC injection current is 110 mA.

where $v_{\max} = 2.73$ V, and $a = -30.4 \mu s^{-2}$. The parameters are optimized using the same error-minimizing iterative procedure. The RMSD for the optimal spectral profile is 0.069 mW/GHz (Fig. 2(f)), compared to 0.083 mW/GHz for Fig. 2(b) and 0.081 mW/GHz for Fig. 2(d).

We then measure the SBS gain profiles produced by the spectral broadened pump beam using the current modulation waveforms depicted in Fig. 1(g) (the “fast” modulation) and Fig. 2(e) (the “slow” modulation). The experiment setup is shown in Fig. 3. To independently measure the SBS gain profile, we use a weak unmodulated monochromatic signal beam (input power P_{s0}), and record the amplified signal beam power P_s at the photoreceiver as we slowly scan the frequency of the signal beam. The SBS power gain G is given by

$$G = \ln(P_s/P_{s0}). \quad (2)$$

The SBS power gain G is related to $g(\omega_s)$ by $G(\omega_s) = g(\omega_s)L_{eff}$, where $L_{eff} = (1 - e^{-\alpha L})/\alpha = 1.64$ km is the effective length of the fiber, $L (= 2$ km) is the physical length of the fiber and $\alpha (= 0.9$ dB/km) is the attenuation coefficient of the fiber.

Figure 4(a) shows the measured SBS gain G profiles for the fast and slow modulation methods. As discussed previously, the SBS gain profile is the convolution of the pump spectrum with the intrinsic narrow Lorentzian lineshape. In our case where the pump spectrum bandwidth (5 GHz) is much larger than the narrow Lorentzian linewidth (~ 52 MHz in HNLFF), the resultant SBS gain profile is similar to the pump spectrum, as seen in Fig. 4(a). We see that the SBS gain profile is not as sharp on the edges using the fast noise-modulation waveform, which is due to the fluctuating temperature, as discussed above. On the other hand, the slow triangular-like waveform results in a deterministic value of the laser temperature at any moment. Therefore, the frequency of the laser is well-defined at the edge of the modulation waveform. However, this is not true for the fast noise modulation, where the temperature is affected by the previous history of the modulation and thus has wide fluctuations. However, as shown next, the reduced slope of the edges for the fast noise modulation does not substantially affect its slow light performance.

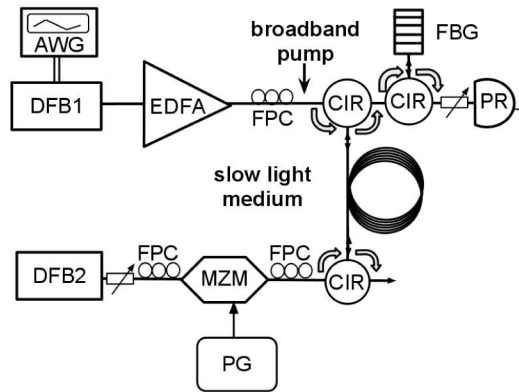


Fig. 3. Experiment setup. Spectrally broadened pump and signal beams counter-propagate in the 2-km-long slow light medium (HNLF, OFS Inc.), where they interact via the SBS process. The SBS frequency shift in HNLF is 9.62 GHz. A fiber Bragg grating (FBG, bandwidth 0.1 nm) is used to filter out the Rayleigh backscattering of the pump beam from the amplified and delayed signal pulse sequence before detection. AWG: arbitrary function generator (Tektronix AFG3251), DFB1: 1550-nm DFB laser diode (Sumitomo Electric, STL4416), EDFA: erbium doped fiber amplifier (IPG Photonics EAD 1K), DFB2: 1550-nm DFB laser diode (Fitel FOL15DCWC), MZM: Mach-Zehnder Modulator, PG: electronic signal pattern generator, PR: 12 GHz photo-receiver (New Focus 1544b), FPC: fiber polarization controllers, CIR: optical circulator.

3. Slow-light performance

We next compare the delay performance of the fast and slow modulation methods. First, we use a continuous-wave signal beam ($P_{s,0} = 48 \mu\text{W}$) that is tuned to the SBS resonance to measure the line center SBS gain G at different pump powers. Again, G is obtained from Eq. (2). As shown in Fig. 4(b), both modulation formats result in identical linear growth of G with respect to the pump power P_p when it is low. As P_p increases, we see that the slow modulation method results in an early saturation in comparison to the case for the fast modulation waveform. Saturation takes place when the SBS gain G is large enough so that a great portion of the power in the

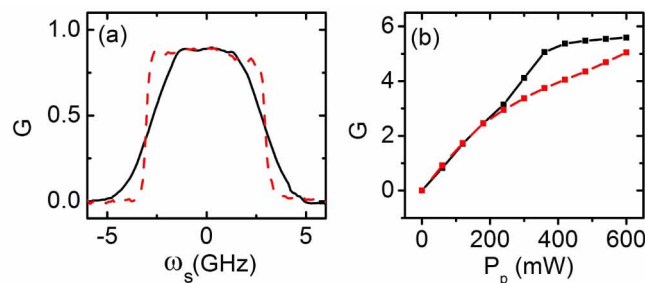


Fig. 4. (a) SBS gain profiles for fast (solid black line) and slow modulations (red dashed line) at $P_p = 70 \text{ mW}$. (b) SBS gain saturation for fast and slow modulation methods. The black solid line shows the SBS gain G for the fast noise modulation, which grows linearly with pump power P_p until saturated. The red dashed line shows the SBS gain G for the slow modulation, which starts to saturate gradually at a much smaller P_p compared to the fast modulation method.

pump beam is transferred into the signal beam, and the exponential amplification of the signal beam cannot be sustained [20].

The early saturation in the slow modulation case is likely due to fluctuations in G . The fluctuation in G is related to the uneven frequency swept rate and the end effect. In the slow modulation method, the frequency of the pump beam is slowly swept. During the modulation period of $2.5 \mu\text{s}$, a monochromatic signal beam is only intermittently amplified during the short time period when the pump-probe frequency difference is equal to the SBS frequency shift within the resonance linewidth. An estimate of the average interaction time period gives $52 \text{ MHz}/5 \text{ GHz} \times 2.5 \mu\text{s} = 26 \text{ ns}$. On this time scale, sweep rate fluctuations result from the short thermal constants of the DFB laser can significantly affect the length of the interaction time period and give rise to fluctuations in G . Moreover, since the SBS amplification process in the slow modulation method is intermittent, there is an end effect that induces more fluctuations in G . In our experiment specifically, the frequency of the pump beam as seen by the signal beam goes through a little less than 8 periods of modulation during the whole propagation time ($\sim 9.7 \mu\text{s}$) through the 2-km-long HNLF. Since the number of modulation periods during the propagation time is not an exact integer, the signal beam can meet the resonant pump frequency for different times (7 or 8), depending on the relative time when we measure the waveform during the modulation period. As a result of both effects, the output signal beam measured at some particular time is amplified more than others and is more likely to saturate the gain. This behavior results in the gradual early saturation seen in Fig. 4(b).

In the fast modulation method, on the other hand, a monochromatic signal is constantly amplified by the frequency-matching component in the broadband pump beam as it travels through the fiber. Pump beam frequency chirping rate might still have uncontrolled jitter on a faster time scale beyond 400 MHz, but the SBS interaction cannot response to such fast processes. The output signal amplification results from the accumulated SBS interaction through the whole fiber. Therefore, G is uniform and stable in this case. The fluctuation in G for the slow modulation method is the source of the low-frequency fluctuations that degrades the fidelity of a data waveform.

The small number of scanning periods in the 2-km-long HNLF can be increased by substantially increasing the fiber length while keep the modulation rate slow. For this reason, in our experiment, a 20-km LEAF fiber is used for the slow light fidelity check in a long fiber. By doing that, we expect to reduce the fluctuations due to the end effect and provide more averaging along the fiber that can help reduce G fluctuation and stabilize the output signal. However, as shown next, a much longer fiber will increase noise from spontaneous Brillouin scattering [21, 22] and boost SBS G saturation, as a result of increased SBS gain coefficient. Also, dispersion of the fiber increases with length, which induces distortion to the signal pulse and degrade the performance. The possible fiber length increase is also limited by practical factors of cost and volume, and it is impossible to use this method to compensate for a modulation rate increase of 1000 as demonstrated in our experiment comparison between the fast and slow modulations.

To measure the delay and fidelity for a data sequence, we use our 5-GHz broadband SBS slow light system to delay a 2^{12} bit-long return-to-zero (RZ) binary data sequence. This data sequence contains all 2^8 8-bit-long sequences separated by 8-bits 0s serving as a buffer. In this arrangement, the pattern-dependent delay is averaged. The use of an RZ signal is more reliable in situations with pulse broadening effects, but takes twice as much bandwidth to achieve the same data rate compared to the non-RZ coding. A data rate of 2.5 Gb/s is used for the signal to match the SBS slow light bandwidth of 5 GHz (FWHM), where the width of a single pulse is equal to 200 ps. The data sequence is generated by a pattern generator (HP70004A) and encoded on the signal beam via the 10-GHz Mach-Zehnder Modulator (MZM). We use a weak

signal seed laser beam (power $P_{s0} = 12 \mu\text{W}$) and restrict $P_p < 500 \text{ mW}$ to avoid SBS gain saturation in HNLf ($P_p < 300 \text{ mW}$ in LEAF). After propagating through the fiber, the delayed and amplified signal beam is detected by a 12-GHz photoreceiver and recorded on an 8-GHz digital sampling oscilloscope (Agilent DSO80804B). Slow light performance for the fast and slow modulation methods is evaluated by the well-known fidelity metrics of EO and SNR based on the eye-diagram of the output signal at various pump power levels.

We first measure the slow light pattern delay by generating the output eye diagram, which is essentially an overlap of the time domain output traces for a certain number of bit periods. The pattern delay is determined by comparing the position of the maximum eye-opening with and without the pump beam. Figure 5(a) shows the measured pattern delay for both the slow and fast pump modulation formats as a function of P_p . Since a weak signal beam is used in the measurement, the measured pattern delay goes linearly with P_p and no significant saturation is observed. Both modulation formats yield the same delay within the measurement error, which agrees well with the theoretical simulation delay time for a rectangular-like optimized gain profile [11] (blue dotted-dash line) and a super-Gaussian gain profile (cyan dash-double dot line). As shown in both experiment data and simulation, the reduced slope of the super-Gaussian gain profile in the fast modulation method does not significantly reduce the delay time. The reason for that could be traced in Fig. 5(b), where we observe the temporal profile of the output signal sequence. Shown in this figure are the averaged pulse profiles at $P_p = 350 \text{ mW}$ for the first “1” in the data sequence, which is an isolated pulse with many bits of “0”s before and after. We see that the delayed pulse shapes for both modulation methods are very close. Compared with the undelayed pulse shape, which is a super-Gaussian, we see that both fast and slow modulation SBS gain profiles re-shape the signal pulse into a Gaussian profile. This is because high temporal frequency components beyond the 5-GHz bandwidth are cut out. Nevertheless, the distortion is small. We can also see that the fast modulation method results in a more symmetric pulse profile, while the slow modulation method produces small ripples behind the main pulse whose profile is asymmetric. The better output pulse profile in the fast modulation method is a result of the smoother phase response for the super-Gaussian shaped gain profile. The asymmetric pulse shape for the slow modulation reduces the peak delay difference between the two methods, resulting in a very close delay performance observed in Fig. 5(a). Based on results shown in Figure 5(a) and (b), we see that both slow and fast modulations demonstrate similar delay and pulse distortion behaviors, allowing us to do the following fidelity performance comparison between these two methods.

Also shown in Fig. 5(a) is the pattern delay in the 20-km LEAF fiber using the slow modulation method. A steeper increase of delay time with P_p is observed as a result of increased Brillouin gain coefficient in the longer fiber. Pump power P_p is restricted within 300 mW to avoid SBS gain saturation.

We next study the signal fidelity of the slow light device. The slow light fidelity metrics are measured in terms of EO and SNR. The EO is measured by the maximum difference between the minimum value of high level and the maximum value of the low level in the eye diagram (shown in Fig. 6). The SNR at the eye-center is defined as the ratio of the EO with the quadratic mean of the standard deviations (noise) of the high and low levels.

Figure 5(c) shows the EO and Fig. 5(d) shows the SNR as functions of P_p . Note that as we change P_p , the power of the signal beams goes through 3-4 orders of magnitude, which is beyond the dynamic range of most photoreceiver. In our experiment, an detection attenuation is set to avoid detector saturation at $P_p = 500 \text{ mW}$ in HNLf ($P_p = 300 \text{ mW}$ in LEAF). As the output signal beam is amplified with increasing P_p , the signal fidelity first increases as the signal overtakes the detector dark noise, then decreases when the SBS gain approaches saturation at high pump power, where amplified spontaneous Brillouin scattering begins to dominate [21].

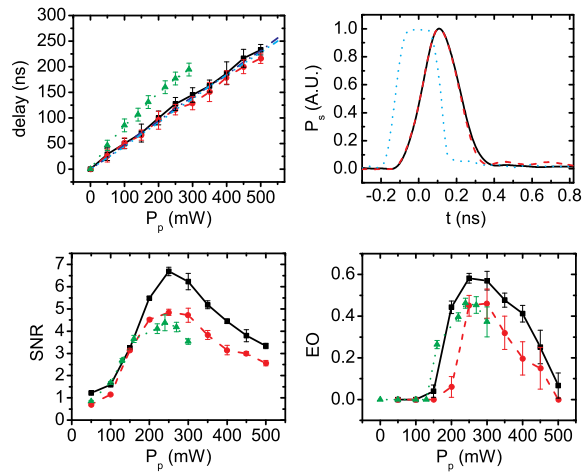


Fig. 5. Slow light performance for fast (solid black line) and slow (dashed red line) modulation waveforms in HNLf, and slow modulation waveform in LEAF (dotted green line). (a) Slow light delay as a function of P_p . The theoretically predicted delay for a rectangular-like optimized gain profile (blue dash-dot line) and for a super-Gaussian gain profile (cyan dash-double dot line) in the HNLf fiber are also shown. SBS gain saturation is avoided using a signal data sequence with a small peak optical power $P_{s0} = 12 \mu\text{W}$; (b) Averaged output signal profiles at $P_p = 350 \text{ mW}$ for the first single pulse in the data sequence, together with the undelayed pulse profile at $P_p = 0 \text{ mW}$ (blue dotted line) in HNLf. Both fast and slow modulation methods result in very similar pulse profile modification without significant broadening. The amplitude of the pulses is normalized as a percentage of the peak pulse height; Fidelity metrics are shown in (c) EO and (d) SNR as functions of P_p , demonstrating better performance for the fast modulation.

Comparing the slow light performance for the fast and slow modulation methods in the HNLf fiber, we see that while both modulation methods result in similar trends for signal quality at different pump power levels, the fast noise-modulation method results in better data fidelity over all pump power levels. In particular, Fig. 6 shows an example of the output eye diagrams for both modulation methods at $P_p = 350 \text{ mW}$, where 50% more EO is obtained for the fast modulation method. A fractional delay (ratio of the delay with the width of a single pulse) of 0.81 with a SNR of 5.2 is achieved at $P_p = 350 \text{ mW}$ for the fast modulation method. Compared to the slow modulation method, the fast modulation method increases the EO by 50% and SNR by 36%, demonstrating significant enhancement of data fidelity with the same delay.

The SNR and EO in the 20-km LEAF fiber using the slow modulation method are also shown in Fig. 5 (c) and (d). We see that the trend of the fidelity curves as a function of P_p in LEAF has the similar shape, but the P_p level corresponding to the high fidelity peak is lower due to a larger Brillouin gain coefficient. In the small P_p ($< 200 \text{ mW}$) region, the LEAF fiber has demonstrated fidelity improvement compared to the HNLf fiber using the slow modulation method. In the high P_p ($> 200 \text{ mW}$) region, as a result of larger spontaneous Brillouin amplification noise, the fidelity of the signal drops down in the LEAF fiber. Overall, the slow light performance in the much longer LEAF fiber demonstrate improvement in the small P_p region, but a much better performance is obtained using the fast modulation method in HNLf at all P_p levels.

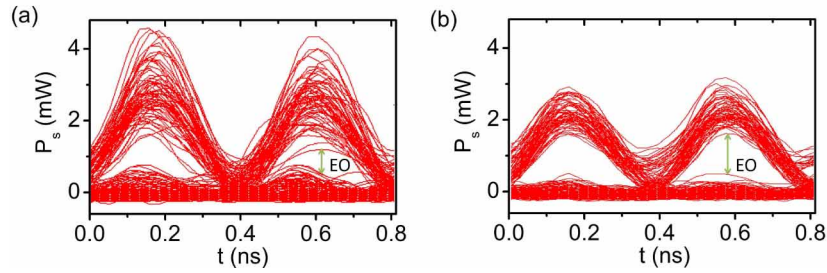


Fig. 6. Eye diagrams of delayed and amplified data sequences for (a) slow and (b) fast modulation waveforms at $P_p = 350$ mW in HNLF. The arrows in the figure show the EO for each case.

4. Conclusion

We have shown that the signal fidelity is significantly improved in a broadband SBS slow light system using noise current modulation of the pump beam spectrum. The SBS gain profile is tailored by controlling the distribution of the noise-modulation waveform. We obtain an optimal flat-topped gain profile using an asymmetric bi-peak-distributed noise-modulation waveform. Using this broadband SBS slow light technique, we significantly improve the signal fidelity compared to previous low-frequency slow synthesized waveform modulation methods. Pattern delays up to 1 pulse width is obtained with high fidelity for RZ data rate of 2.5 Gb/s.

Acknowledgements

We gratefully acknowledges the financial support of the DARPA Defense Sciences Office Slow Light project.